Cancer Research

miR-34a and *miR-34b/c* Suppress Intestinal Tumorigenesis

Longchang Jiang[1] and Heiko Hermeking[1,2,3]

Abstract

The p53-inducible *miR-34a* and *miR-34b/c* genes are frequently silenced in colorectal cancer. To address the *in vivo* relevance of *miR-34a/b/c* function for suppression of intestinal tumor formation, we generated $Apc^{Min/+}$ mice with deletions of the *miR-34a* and/or *miR-34b/c* genes separately or in combination. Combined deletion of *miR-34a/b/c* increased the number of intestinal stem cells as well as Paneth and Goblet cells, resulting in enlarged intestinal crypts. *miR-34a/b/c*-deficient $Apc^{Min/+}$ mice displayed an increased tumor burden and grade and decreased survival. *miR-34a/b/c*-deficient adenomas showed elevated proliferation and decreased apoptosis and displayed pronounced bacterial infiltration, which may be due to an observed decrease in infiltrating immune cells and downregulation of barrier proteins. mRNA induction in *miR-34a/b/c*-deficient tumors was enriched for miR-34a/b/c seed-matching sites and for mRNAs encoding proteins related to epithelial–mesenchymal transition, stemness, and Wnt signaling. Accordingly, cells explanted from *miR-34a/b/c*-deficient adenomas formed tumor organoids at an increased rate. Several upregulated miR-34 targets displayed elevated expression in primary human colorectal cancers that was associated with lymph-node metastases (*INHBB*, *AXL*, *FGFR1*, and *PDFGRB*) and upregulation of *INHBB* and *AXL* in primary colorectal cancer was associated with poor patient survival. In conclusion, our results show that *miR-34a/b/c* suppress tumor formation caused by loss of *Apc* and control intestinal stem cell and secretory cell homeostasis by downregulation of multiple target mRNAs. *Cancer Res; 77(10); 2746–58. ©2017 AACR.*

Introduction

Colorectal cancer is a leading cause of cancer death. In the United States alone, 134,490 new cases and 49,190 deaths from colorectal cancer were expected in 2016 (1). Colorectal cancer is a multistep process driven by mutational activation of several oncogenes and genetic/epigenetic inactivation of tumor suppressors (2). The majority of colorectal cancers originate from benign adenomas, which are caused by inactivating mutations in the *adenomatous polyposis coli (APC)* gene. *APC* mutation leads to the constitutive activation of the Wnt/β-catenin pathway, which results in the increased expression of β-catenin, a critical regulator of intestinal epithelial cell homeostasis (3). During colorectal cancer progression, additional mutations in key oncogenes and tumor suppressor genes, such as *p53*, are acquired. $Apc^{Min/+}$ mice inherit a mutant *Apc* allele that results in a truncation of the APC protein at amino acid 850 (4) and spontaneously lose the wild-type *Apc* allele, resulting in multiple benign adenomas mainly throughout the small intestine (5). Thus, $Apc^{Min/+}$ mice allow to study the influence of putative tumor suppressor genes on the initiation of intestinal tumorigenesis *in vivo* (6).

The tumor suppressor gene *p53* is inactivated in the majority of colorectal cancers and encodes a transcription factor, which is posttranscriptionally induced by DNA damage and a number of additional cellular stresses (7). Besides regulating the expression of mRNAs, p53 also controls the expression of noncoding RNAs, such as lncRNAs and microRNAs (miRNA; refs. 8, 9). Many tumor suppressive functions of p53 are thought to be mediated by p53-induced miRNAs (8, 10). Among the p53-induced microRNA-encoding genes, *miR-34a* and *miR-34b/c* display the most consistent and pronounced induction, which may explain why they were identified as one of the first p53-regulated miRNAs (11).

Via downregulation of key-regulators, miR-34a/b/c suppress numerous cancer-associated processes, such as cell proliferation and survival (12), epithelial–mesenchymal transition (EMT; ref. 13), and stemness (14). Moreover, miR-34a/b/c presumably function as cell-fate determinants in colonic cancer stem cells (CSC) by suppressing Notch activity (15). Furthermore, miR-34a/b/c regulate the homeostasis of normal stem cells (16) and suppress the formation of induced pluripotent stem cells (IPSCs) (17).

Consistent with a tumor suppressive role in tumorigenesis, downregulation of *miR-34a/b/c* expression has been observed in a variety of human cancers (8). *miR-34a/b/c* expression is also epigenetically silenced by CpG methylation in colorectal cancer cell lines (18) and in primary colorectal cancers (19). These findings suggest an important role of miR-34a/b/c as downstream effectors of p53 and potential tumor suppressors in colorectal cancer. In line with its tumor suppressive potential miR-34a mimetics are currently tested in the clinics for treatment of advanced cancer (20).

Here, we report the generation of $Apc^{Min/+}$ mice carrying targeted deletions of the *miR-34a* and *miR-34b/c* genes and the characterization of the resulting phenotypes at the organismal

[1]Experimental and Molecular Pathology, Institute of Pathology, Ludwig-Maximilians-University, München, Germany. [2]German Cancer Consortium (DKTK), Partner site Munich, Munich, Germany. [3]German Cancer Research Center (DKFZ), Heidelberg, Germany.

Note: Supplementary data for this article are available at Cancer Research Online (http://cancerres.aacrjournals.org/).

Corresponding Author: Heiko Hermeking, Ludwig-Maximilians-University München, Thalkirchner Strasse 36, Munchen D-80337, Germany. Phone: 11-49-2180-73685; Fax: 11-49-89-2180-73697; E-mail: heiko.hermeking@med.uni-muenchen.de

doi: 10.1158/0008-5472.CAN-16-2183

and molecular level. Our findings provide genetic proof of a tumor suppressive function of the *miR-34a* and *miR-34b/c* genes during intestinal tumorigenesis.

Materials and Methods

Animals

The generation of *miR-34a*$^{-/-}$ mice with a C57BL6/SV129 background has been described previously (21). *miR-34b/c*$^{fl/fl}$ mice were kindly provided by Dr. Alexander Nikitin (Cornell University, Ithaca, NY; ref. 16). In brief, gene-specific deletions were generated by using homologous recombination with a vector containing *miR-34a* or *miR-34b/c* sequences flanked by *loxP* sites and an intronic Neomycin resistance (*Neo*) cassette flanked *frt* sites individually (21). The *Neo* cassette was removed by crossing with *flp*-mice and germline *miR-34a* or *miR-34b/c* knock-out mice were generated by crossing with *CMV-Cre* mice. *miR-34a*$^{-/-}$; *b/c*$^{-/-}$ compound mice were generated by crossing *miR-34a*$^{-/-}$ and *miR-34b/c*$^{-/-}$. The resulting genotypes were obtained in the expected Mendelian ratios and the offspring displayed no overt phenotype. *miR-34a*$^{-/-}$, *miR-34b/c*$^{-/-}$, *miR-34a*$^{-/-}$; *miR-34b/c*$^{-/-}$ and *miR-34a*$^{+/+}$; *miR-34bc*$^{+/+}$ mice were crossed with *Apc*$^{Min/+}$ mice to obtain mice with the following genotypes: *miR-34a*$^{-/-}$; *Apc*$^{Min/+}$, *miR-34b/c*$^{-/-}$; *Apc*$^{Min/+}$, *miR-34a/b/c*$^{-/-}$; *Apc*$^{Min/+}$, and *miR-34a/b/c*$^{+/+}$*Apc*$^{Min/+}$. Mice were housed in individually ventilated cages (IVC). Animal studies were approved by the Government of Upper Bavaria, Germany (AZ 55.2-1-54-2532-4-2014).

Tissue preparation and tumor count

Mice were sacrificed at 18 weeks of age. Whole intestines were isolated, separated into four equal parts, flushed with PBS, opened longitudinally, photographed, and fixed as Swiss rolls in 4% buffered formaldehyde. Tumor numbers and size were evaluated using ImageJ software.

Histology and IHC

Three-micron paraffin sections were used for hematoxylin and eosin staining and periodic acid–Schiff (PAS) staining according to standard protocols. Tumors from *Apc*$^{Min/+}$ mice were classified as adenomas with either low- or high-grade dysplasia, based on nuclear-cytoplasmic ratio, nucleus location, prominence of nucleoli, gland architecture, amount of interglandular stroma, and the presence of mucus secretion. Immunohistochemistry was performed using antibodies and reagents listed in Supplementary Table S1. For each immunohistochemical detection $\geq$ 40 tumors per genotype were examined. Positive staining was evaluated by Image-Pro plus and ImageJ software.

In situ hybridization and fluororescence *in situ* hybridization

For detection of intestinal stem cells an *Olfm4*-specific, DIG-labeled RNA probe was generated using a murine *Olfm4* vector (kindly provided by Dr. Hans Clevers, Hubrecht Institute, Utrecht, The Netherlands) in combination with a DIG Northern Starter Kit (Roche Diagnostics). *in situ* hybridization (ISH) was performed as described (22). To visualize intestinal bacteria by fluorescence *in situ* hybridization, the universal eubacteria probe (EUB338) and negative control probe (NON338) were employed. The 5′-FITC-labeled EUB338 DNA (5′-GCTGCCTCCCGTAGGAGT-3′) and 5′-Cy3-labeled NON338 DNA (5′-CGACGGAGGGCATCCTCA-3′) probes were synthesized by Metabion (Planegg) and hybridized to 3-μm paraffin sections.

Transcriptomic analysis

Total RNA from tumors was isolated using the RNeasy Plus Mini Kit (Qiagen) with an on-column DNase digestion (three RNA samples per genotype; each tumor RNA sample represented a pool of 3 tumors isolated from the same mouse). Random primed cDNA libraries were generated and sequenced using the HiSeq2500 (Illumina) platform by GATC (Konstanz). Each sample was covered by at least 35 million single reads of 50 bp length. Data were normalized in R with the RUVSeq (23) module and differential expression analysis was performed using Chipster (24). The overlap of DEseq2 and edgeR results were considered to represent the most significantly, differentially expressed genes. Gene Ontology (GO) and KEGG pathway analysis was performed with DAVID Bioinformatics Resources (25). Gene Set Enrichment Analysis (GSEA) was performed using the GSEA (26) software. miR-34a/b/c targets were predicted with TargetScan 6.2 (27). Expression data were deposited in the Gene Expression Omnibus website (accession no. GSE84138).

Cell lines and culture, generation of cell pools with conditional *pri-miR-34a* expression, and tumor organoid culture

H1299 lung cancer cells used for 3′-UTR reporter assays were from own stocks and their negativity for p53 was validated. SW620 colorectal cancer cells used for ectopic *pri-miR-34a* expression were from own stocks and authenticated by STR analysis in 2014 (Eurofins Medigenomix Forensik GmbH, Ebersberg, Germany). H1299 and SW620 cancer cell lines were kept in Dulbecco's modified Eagle's medium (DMEM) and 10% fetal calf serum (Invitrogen) at 5% CO_2. SW620 cells were transfected with episomal pRTR-*pri-miR-34a* expression plasmids as described before (13). After 24 hours, cell pools were selected by addition of puromycin (2 μg/mL) for 10 days. GFP expression was evaluated by fluorescence microscopy 48 hours after addition of 100 ng/mL doxycycline (DOX) to the cell pools. Intestinal adenoma cells from *Apc*$^{Min/+}$ mice were isolated and counted using a hemocytometer. Single cells (15,000) were embedded in 50 μL Matrigel per well in 24-well plates. The tumor organoid culture medium was formulated as described before (28).

3′-UTR reporter assays

The 3′-UTR of *Wasf1* was PCR amplified from genomic DNA isolated from mouse tissue, inserted into pGL3-control-MCS vector downstream of a firefly luciferase ORF, and verified by sequencing. H1299 cells were seeded in a 12-well plate with 3×10^4 cells/well and transfected with 100 ng of pGL3-*Wasf1* plasmid, 20 ng of *Renilla* reporter plasmid for normalization, and 25 nmol/L *miR-34a* or *miR-34c* pre-miRNAs or a negative control oligonucleotide (Ambion). Forty-eight hours later, luciferase assays were performed with the Dual-Luciferase Reporter 1000 Assay System (Promega). Fluorescence intensities were measured with an Orion II Microplate Luminometer (Titertek-Berthold). Primers used for cloning and sequencing are listed in Supplementary Table S2.

Quantitative real-time PCR and Western blot analysis

Total RNA was isolated from tumor samples or cultured cell lines using the RNeasy Plus Mini Kit (Qiagen). cDNA was generated by Verso cDNA kit (Thermo Scientific) and quantitative real-time PCR (qPCR) was performed by using Fast SYBR Green Master Mix (Applied Biosystems) and a LightCycler 480 II (Roche Diagnostics). Relative gene expression was determined using the

$2^{-\Delta\Delta C_t}$ method (29). The individual mRNA levels were normalized to β-actin. Primers used for qPCR are listed in Supplementary Table S3.

For protein lysates tumor samples or cultured cells were lysed in RIPA buffer containing cOmplete Mini protease inhibitor cocktail tablets (Roche Diagnostics). Lysates were sonicated and centrifuged. Whole-lysate proteins (30–60 μg) were loaded per lane. Gel electrophoresis and transfer to PVDF membranes (Millipore) were carried out using standard protocols (Bio-Rad Laboratories). Primary antibodies (Supplementary Table S1) were used in combination with HRP-coupled secondary antibodies. ECL (Millipore) signals were recorded with a 440CF imaging system (Kodak).

Analysis of online expression data sets

The Cancer Genome Atlas (TCGA; ref. 30) gene expression data and follow-up information of colon adenocarcinomas (COAD) were downloaded from NCI's Genomic Data Commons website (GDC; https://gdc.cancer.gov/). Normalized RSEM counts were used to determine the expression of relevant mRNAs. Clinical outcome data were divided into high, intermediate, and low expression groups according to the expression value of individual genes.

Statistical analysis

A two-tailed Student *t* test was used to compare continuous variables. Categorical variables were compared using the χ^2 method. Kaplan-Meier calculations were used to display the overall survival time and the results were compared with a log-rank test. The Sidak method was used to adjust *P* values when multiple comparisons were performed. *P* values less than 0.05 were considered significant and indicated by asterisks (*, $P<0.05$; **, $P<0.01$; or ***, $P < 0.0001$). Univariate, age/gender/tumor grade-adjusted hazard ratios, and 95% confidence intervals (CI) were estimated with a Cox's proportional hazard model. Prism 6 (GraphPad software) or SPSS (IBM) programs were used for calculations.

Results

miR-34a/b/c deletion modulates the architecture of the small intestine in mice

We generated mice carrying deletions of the *miR-34a* or *miR-34b/c* loci and combinations of these. Deletion of *miR-34a*, *miR-34b/c*, or *miR-34a/b/c* in the germline did not significantly influence the lifespan of mice (Fig. 1A). However, we observed a gender-independent increase in the width and depth of crypts of the small intestine in *miR-34a/b/c*-deficient mice, which presumably caused the minor increase in the total length of the small intestine (Fig. 1B). Notably, the numbers of Paneth cells per crypt and Goblet cells per villus were significantly increased in *miR-34a/b/c*-deficient mice (Fig. 1C and D). In addition, the frequency of stem cells at the crypt base was significantly increased in *miR-34a/b/c*-deficient mice as determined by detection of the stem cell marker *Olfm4* using *in situ* hybridization (Fig. 1E). These phenotypes were independent of the gender (Fig. 1B–E).

In order to determine, whether inactivation of *miR-34* genes affects intestinal tumor formation, we generated $Apc^{Min/+}$ mice with deletions of *miR-34a*, *miR-34b/c*, or *miR-34a/b/c*. Also in $Apc^{Min/+}$ mice deficiency for *miR-34a/b/c* resulted in an increase of the number of Paneth, Goblet, and *Olmf4*-positive cells per crypt in untransformed tissue of the small intestine (Supplementary Fig. S1A–D). Similarly, the width and depth of the crypts were increased significantly in *miR-34a/b/c*-deficient $Apc^{Min/+}$ mice, but the minor increase in the length of the small intestine was not statistically significant (Supplementary Fig. S1E). Again, these architectural changes were observed in both, male and female mice. Therefore, deletion of one *APC* allele did not influence the morphological changes in the intestine caused by deletion of *miR-34a/b/c*.

miR-34a/b/c loss enhances tumorigenesis in $Apc^{Min/+}$ mice

Notably, *miR-34a/b/c*$^{-/-}$; $Apc^{Min/+}$ mice showed signs of morbidity sooner and exhibited a shorter life-span than wild-type $Apc^{Min/+}$ mice (Fig. 2A). In contrast, $Apc^{Min/+}$ mice deficient for either the *miR-34a* or the *miR-34b/c* allele did not show a statistically significant change in life-span (Fig. 2A). When mice were sacrificed at the age of 18 weeks and the entire small intestinal tract was examined, *miR-34a/b/c*$^{-/-}$; $Apc^{Min/+}$ and, to a lesser extent, *miR-34a*$^{-/-}$; $Apc^{Min/+}$ knockout mice showed a significantly increased number of tumors when compared with $Apc^{Min/+}$ mice (Fig. 2B and C). Furthermore, the total tumor area in *miR-34a/b/c*$^{-/-}$; $Apc^{Min/+}$ mice was ∼4 times larger than in wild-type $Apc^{Min/+}$ mice (Fig. 2D). The frequency of large tumors (>6 mm^2) was significantly higher when *miR-34a/b/c*, but not when only *miR-34a* or *miR-34b/c* genes had been deleted in $Apc^{Min/+}$ mice (Fig. 2E). We also noted a significantly increased number of adenomas with high-grade dysplasia in *miR-34a/b/c*-deficient $Apc^{Min/+}$ mice, whereas the inactivation of either *miR-34a* or *miR-34b/c* alone did not have this effect (Fig. 2F). Taken together, our findings show that the inactivation of *miR-34a/b/c* promotes intestinal tumor formation by increasing tumor initiation and enhancing the growth of tumors in $Apc^{Min/+}$ mice. As the combined inactivation of *miR-34a* and *miR-34b/c* genes was necessary for these effects, these miRNAs may have overlapping functions and compensate each other. In addition, these results are in accordance with the combined epigenetic inactivation of *miR-34a* and *miR-34b/c* by DNA methylation, which has been detected in more than 75% of analyzed colorectal cancer samples (31). In the subsequent analyses, we therefore focused on studying mice with simultaneous deletion of *miR-34a* and *miR-34b/c*.

miR-34a/b/c loss affects proliferation, apoptosis, and infiltration by bacteria and immune cells of adenomas

Notably, tumors in *miR-34a/b/c* knockout $Apc^{Min/+}$ mice showed a significant increase in proliferation and a significantly reduced rate of apoptosis (Fig. 3A). The frequency of stromal cells within the tumors was not affected by *miR-34a/b/c* deletion as determined by detection of vimentin. Because it was recently shown that bacterial infiltration promotes tumorigenesis in $Apc^{Min/+}$ mice (32), we asked whether *miR-34a/b/c* deletion affects the presence of bacteria in intestinal tumors. By detection of bacterial 16S rRNA, we found that adenomas from *miR-34a/b/c*$^{-/-}$; $Apc^{Min/+}$ mice display extensive bacterial infiltration regardless of tumor size (Fig. 3A) or tumor grade (Supplementary Fig. S2A). However, the adjacent normal intestinal epithelium of all mice analyzed here was devoid of bacteria. Therefore, miR-34a/b/c-deficient mice do not display a general intestinal barrier defect. Unexpectedly, the frequency of immune cells, such as macrophages, T- and B-cell, was decreased in *miR-34a/b/c*-deficient adenomas (Fig. 3B; Supplementary Fig. S2B). Therefore, the increased bacterial infiltration of adenomas may be due to a defect in the tumor-associated immune defense in *miR-34a/b/c*-deficient mice.

Expression profiling of *miR-34a/b/c*-deficient adenomas

To further illuminate the mechanisms by which *miR-34a/b/c* loss promotes intestinal tumorigenesis in $Apc^{Min/+}$ mice, we

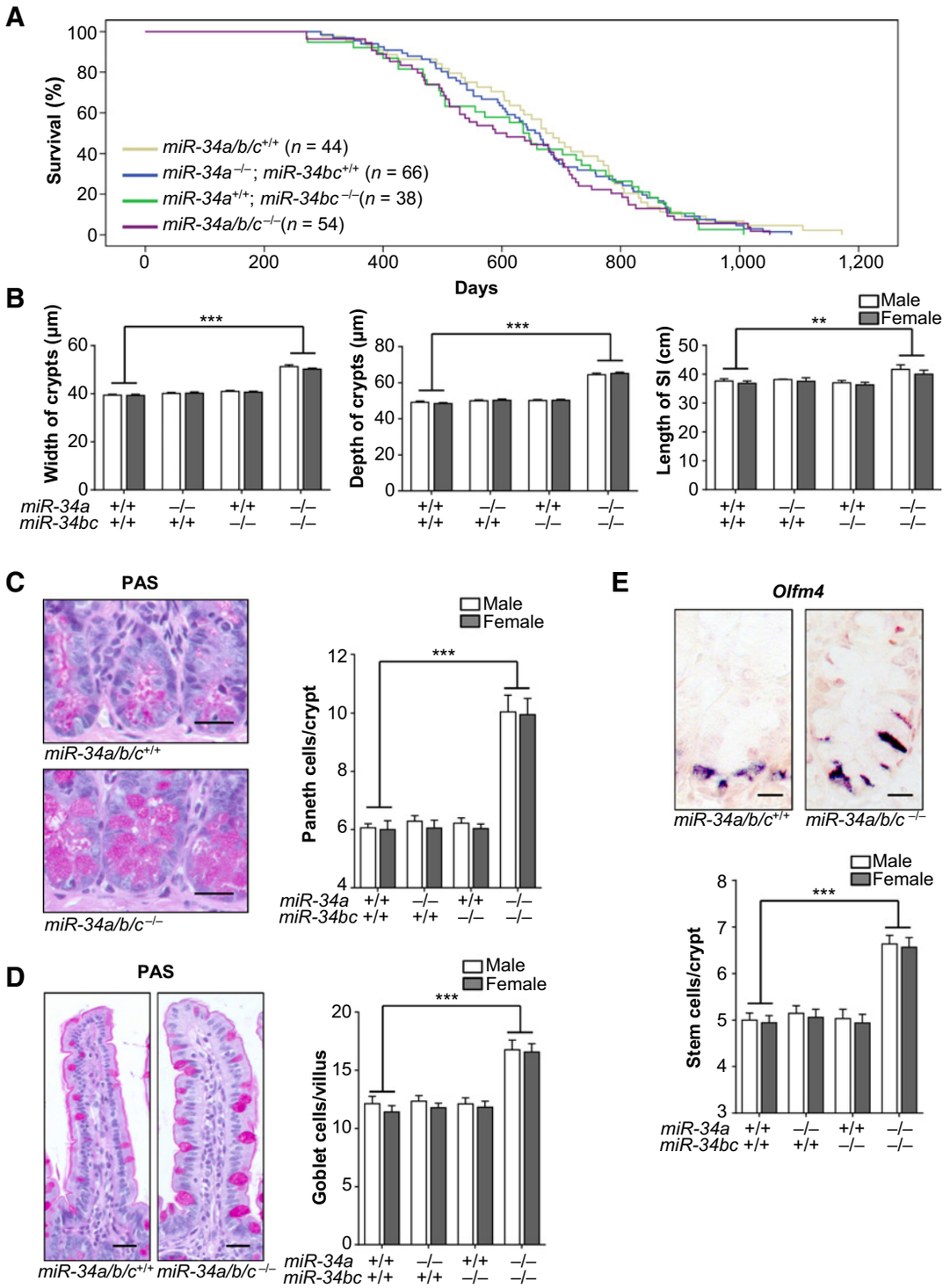

Figure 1.

Effects of *miR-34a/b/c* deletion on the cellular composition of the small intestine in mice. **A,** Kaplan–Meier survival analysis of mice with the indicated genotypes. Results were compared with a log-rank test. **B,** Determination of the width (left graph) and depth (middle graph) of small intestinal crypts. At least 200 crypts in the jejunum from 18-week-old mice were analyzed. The length (right graph) of the small intestine was determined in mice with the indicated genotypes (n $\geq$ 3 mice per gender). **C** and **D,** After PAS-staining Paneth cell number per crypt (**C**) and Goblet cell number per villus (**D**) were evaluated in $\geq$ 50 crypts and $\geq$ 50 villi per mouse, respectively ($n \geq 3$ mice per gender). Scale bar, 25 μm. **E,** Representative pictures of *in situ* hybridization of *Olfm4*-positive cells in the crypts from indicated genotypes. At least 50 crypts per mouse were counted ($n \geq 3$ mice per gender). Scale bar, 10 μm. In **B–E**, n $\geq$ 6 mice per genotype, results are presented as mean ± SEM. **, $P < 0.01$; ***, $P < 0.001$ (Student *t* test).

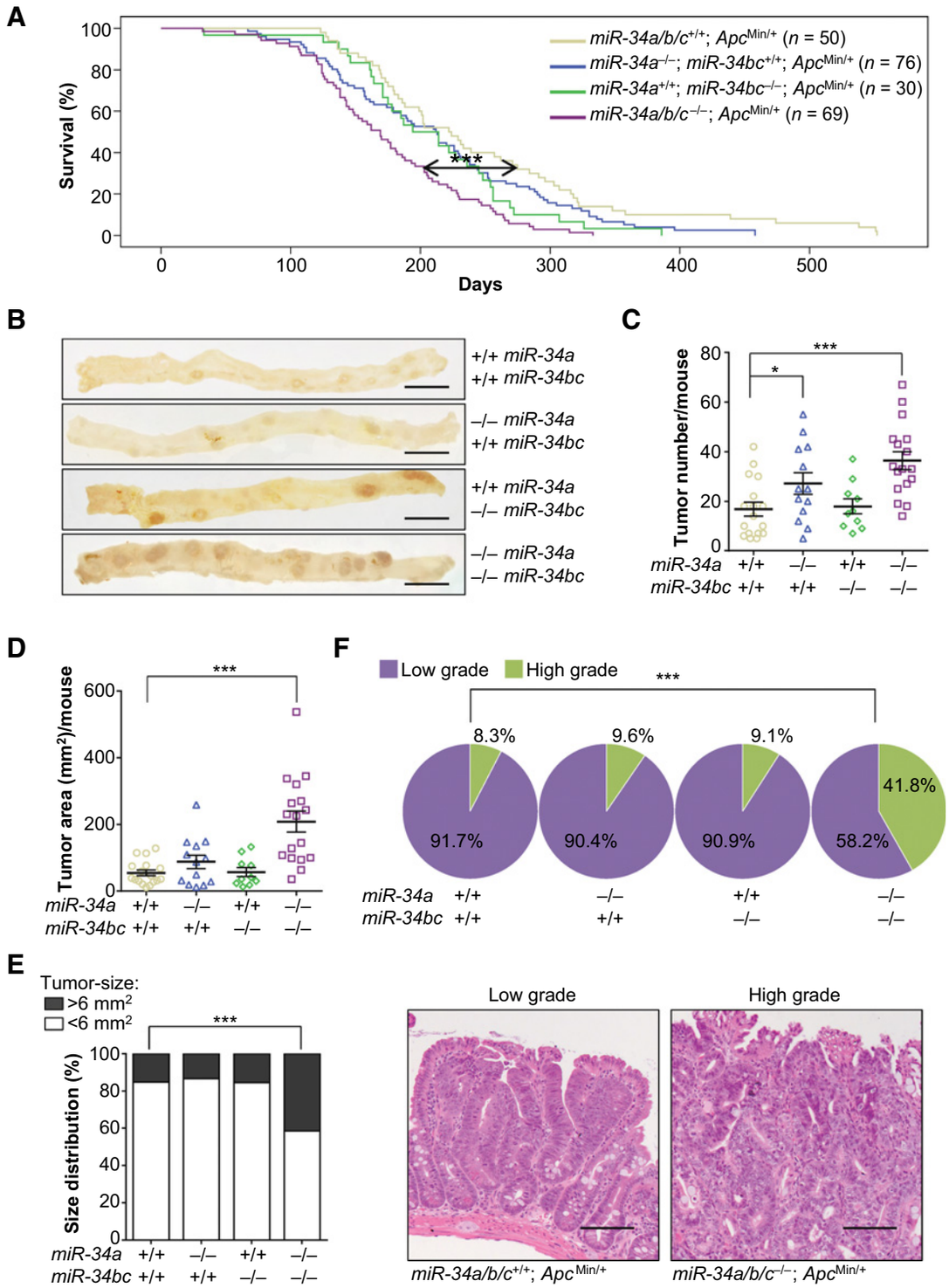

Figure 2.
Effects of *miR-34a/b/c* deletion on tumor characteristics and survival of $Apc^{Min/+}$ mice. **A,** Kaplan–Meier survival analysis of the indicated genotypes. Results were compared with a log-rank test. **B,** Representative images of resected small intestines. Scale bar, 1 cm. **C** and **D,** Quantification of intestinal tumor number (**C**) and tumor area (**D**) per mouse ($n \geq 10$ mice per genotype). **E,** Graph showing the percentage of tumor size (surface area) distribution in ≥ 100 tumors ($n \geq 10$ mice per genotype). **F,** Top, tumor stage (low grade adenoma, high-grade adenoma) of ≥ 66 intestinal tumors ($n \geq 10$ mice per genotype). Bottom, representative images of low- and high-grade adenomas. Scale bar, 100 μm. In **B–F**, tumors from 18 weeks old $Apc^{Min/+}$ mice with the indicated genotypes were analyzed and results are presented as mean ± SEM. *, $P < 0.05$; ***, $P < 0.001$ (Student *t* test).

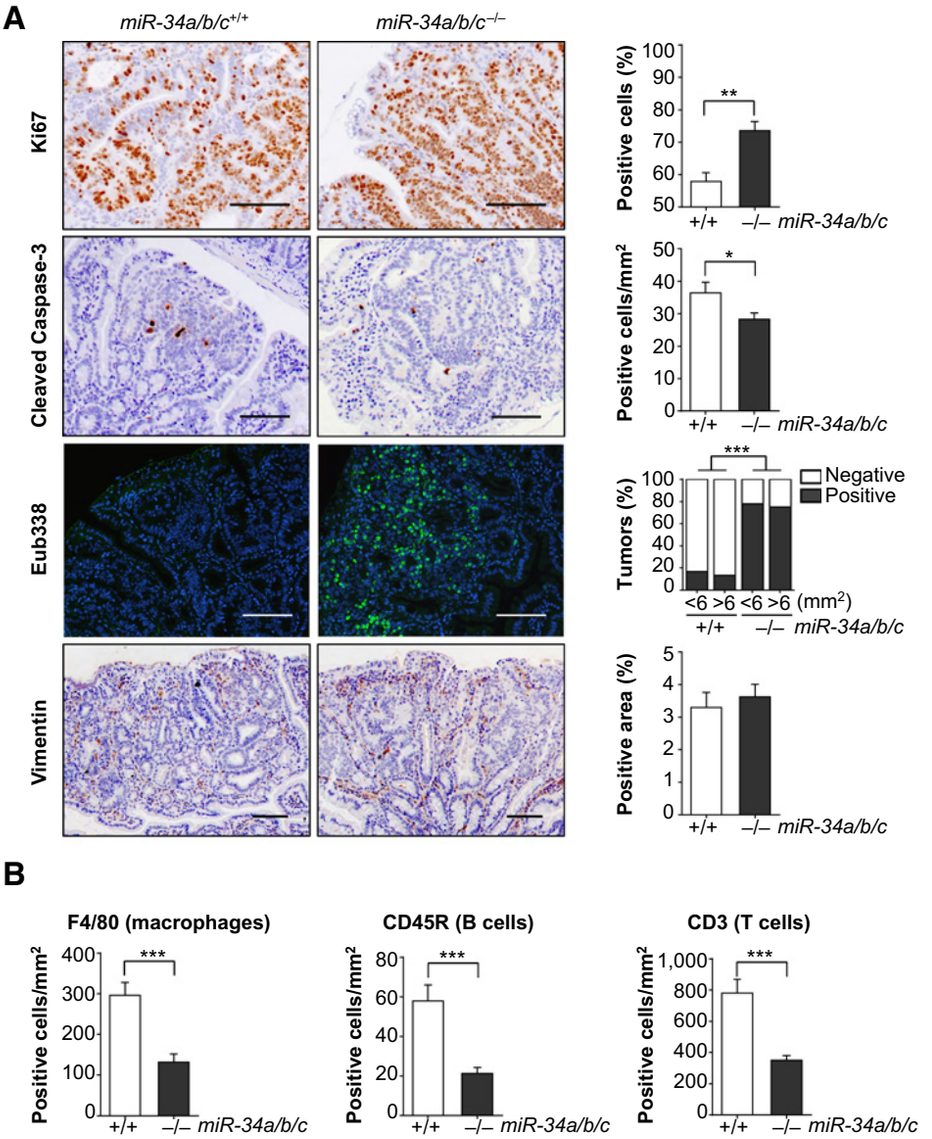

Figure 3.
Effects of *miR-34a/b/c* deletion on proliferation, apoptosis, bacterial infiltration, and stromal cells of $Apc^{Min/+}$ adenomas. Adenomas from 18 weeks old $Apc^{Min/+}$ mice with the indicated genotypes were subjected to several different immunodetections ($n = 7$ mice per genotype). **A,** IHC detection of Ki67, cleaved caspase-3 and vimentin as indicated and fluorescence *in situ* hybridization of universal eubacteria probe (EUB338). Scale bar, 100 μm. **B,** Quantification of infiltrated macrophages, B and T cells by F4/80, CD45R, and CD3 immunodetection, respectively, in adenomas. Results are presented as mean ± SEM. *, $P < 0.05$; **, $P < 0.01$; ***, $P < 0.001$ (Student *t* test).

obtained mRNA expression profiles of adenomas from 18-week-old *miR-34a/b/c*-deficient $Apc^{Min/+}$ mice and wild-type $Apc^{Min/+}$ mice. For each mouse ($n = 3$ per genotype), RNAs derived from three different tumors were pooled, libraries were generated and subjected to RNA-Seq to obtain more than 35 million reads per library. Thereby, we detected the upregulation of 1773 mRNAs, when mRNAs with a $\log_2$-fold change ≥ 0.6 and RPKM ≥ 0.25 in *miR-34*a/b/$c^{-/-}$; $Apc^{Min/+}$ mice versus wild-type $Apc^{Min/+}$ mice were included (Fig. 4A). As expected, the percentage of mRNAs upregulated in the *miR-34a/b/c*-deficient tumors was higher for mRNAs harboring miR-34a/b/c seed-matching sequences than for mRNAs lacking these (Fig. 4B). Three hundred and twenty-four mRNAs were identified as differentially regulated due to *miR-34a/b/c* loss when the raw-count methods DESeq2 (33) and edgeR (34) were applied (Fig. 4C). After unsupervised clustering of these differentially expressed genes, one of the *miR-34a/b/c*-deficient tumor samples showed a divergent expression profile, which was presumably due to biological variation (Fig. 4D). Next, we used Gene Ontology (GO) and KEGG pathway analyses to group the differentially expressed transcripts into functional classes. The GO analysis indicated that the upregulated mRNAs are involved in cell adhesion, extracellular matrix, and growth factor binding functions (Supplementary Fig. S3A). The KEGG analysis showed that several pathways were significantly enriched, such as focal adhesion, ECM-receptor interaction, and pathways related to cancer (Supplementary Fig. S3B). On the contrary, both GO and KEGG analyses indicated that the downregulated genes are mainly involved in immune response functions (Supplementary Fig. S4A and S4B). A subsequent Gene Set Enrichment Analysis (GSEA) revealed that *miR-34a/b/c* deletion results in gene expression signatures related to EMT, hypoxia, angiogenesis, inflammatory response, Kras signaling, and apical junction processes (Fig. 4E). Interestingly, the expression signatures of *miR-34a/b/c*-deficient adenomas also showed a significant overlap with signatures of intestinal stem

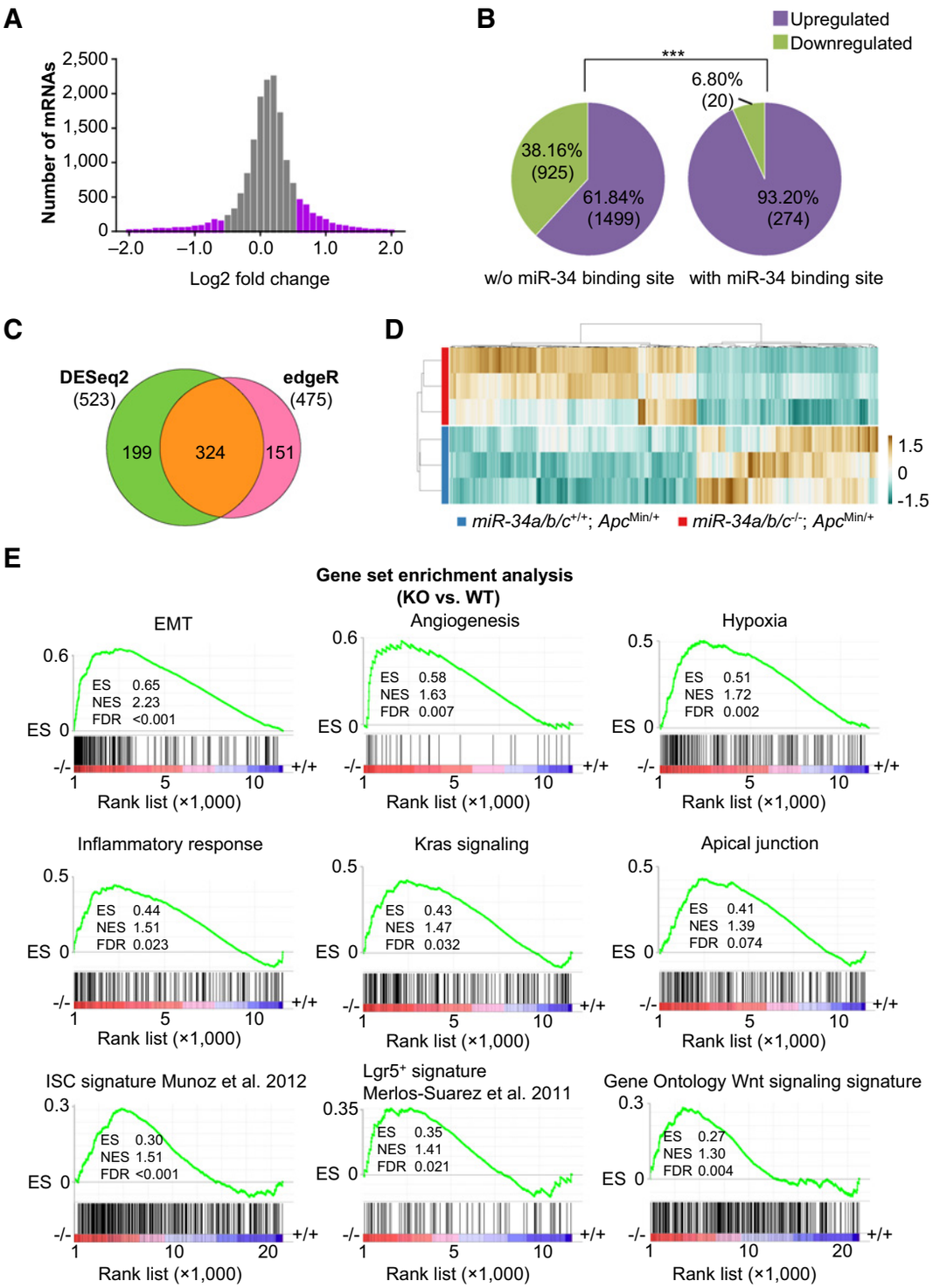

Figure 4.

NGS analysis of *miR-34a/b/c*-dependent mRNA expression in adenomas of $Apc^{Min/+}$ mice. **A,** Results of NGS analysis represented as histogram showing changes in mRNA levels after *miR-34a/b/c* deletion. Transcriptionally regulated genes with a $|\log_2\text{-fold change}| \geq 0.6$ and RPKM ≥ 0.25 are highlighted as purple bars. Fold change denotes the ratio of mRNA expression values in tumors of *miR-34a/b/c*$^{-/-}$; $Apc^{Min/+}$ mice versus *miR-34a/b/c*$^{+/+}$; $Apc^{Min/+}$ mice ($n = 3$ mice per genotype). **B,** Calculation of the percentage of mRNAs differentially regulated in *miR-34a/b/c*-deficient versus wild-type tumors in $Apc^{Min/+}$ mice without (left graph) and with (right graph) *miR-34a/b/c* seed-matching sequences. ***, $P < 0.001$. **C,** Results of DESeq2 and edgeR analyses of the NGS results. **D,** Heatmap of genes with significantly differential expression in tumors from mice with the indicated genotypes. Differential gene expression is shown according to the pseudocolor scale indicated on the right side. **E,** GSEA analysis of mRNA profiles from tumors of *miR-34a/b/c*$^{-/-}$; $Apc^{Min/+}$ mice versus *miR-34a/b/c*$^{+/+}$; $Apc^{Min/+}$ mice.

cells (ISC) (35), Lgr5$^+$ positive cells (36) and the GO Wnt signaling signature. In addition, several regulators of barrier function in IEC were also detected as downregulated by NGS analysis in *miR-34a/b/c*-deficient adenomas (e.g., *Muc1*, *Tff3*, and *Retnlb*; fold change: −4.74, −1.44, and −3.34, respectively). The downregulated mRNA expression of these barrier components was validated by qPCR (Supplementary Fig. S5A). Furthermore, we confirmed the decreased protein expression of MUC1 in *miR-34a/b/c*-deficient adenomas by immunohistochemistry (Supplementary Fig. S5B). The repression of these barrier components may also contribute to the observed infiltration of bacteria into *miR-34a/b/c*-deficient adenomas.

miR-34a/b/c loss enhances the formation of intestinal tumor organoids

To obtain functional evidence for an enhanced stemness of adenoma cells with deletion of *miR-34a/b/c*, we performed a tumor organoid formation assay. Indeed, an increased tumor organoid formation rate was observed for *miR-34a/b/c*-deficient adenoma derived cells when compared with those derived from *miR-34a/b/c*-proficient adenomas (Fig. 5A).

miR-34a/b/c deletion enhances intestinal Wnt signaling in *Apc*$^{Min/+}$ mice

Wnt/β-catenin signaling is critically involved in regulating the homeostasis and neoplastic transformation of the intestine. Because *34a/b/c*-deficient adenomas showed a Wnt signaling signature (Fig. 4E) and the Wnt/β-catenin pathway is directly regulated by miR-34a/b/c (37) and by APC, we determined whether the expression of β-catenin is also affected in the intestinal epithelial cells of *miR-34a/b/c* knockout mice. Interestingly, we detected an increased nuclear accumulation of β-catenin/CTNNB1 protein in normal crypts after *miR-34a/b/c* deletion in *Apc*$^{Min/+}$ mice, but not in *miR-34a/b/c*-deficient wild-type mice (Fig. 5B), indicating that *miR-34a/b/c* deficiency in the presence of hemizygous *Apc* allows the nuclear accumulation of β-catenin in untransformed cells, including the stem cells located at the crypt base, which represent the preferred cells of origin for intestinal adenomas (38). Therefore, this effect of *miR-34a/b/c* loss may explain or at least contribute to the increased rate of tumor initiation in *miR-34a/b/c*-deficient *Apc*$^{Min/+}$ mice.

Validation of miR-34a/b/c target expression

By bioinformatics analyses of the mRNA profiles obtained here, we identified a set of 11 upregulated mRNAs with miR-34 seed-matching sites in their 3′-UTR, which may, at least in part, mediate the tumor suppressive function of miR-34a/b/c (Supplementary Table S4; Fig. 6A). These mRNAs and a selected set of mRNAs with known pro-tumorigenic functions were analyzed by qPCR to exemplarily validate the NGS results (Fig. 6B). Several of these factors have already been characterized as direct miR-34 targets by others and us (*Pdgfra* (39), *Pdgfrb* (39), and *Axl* (40)). In addition, components of the Wnt pathway and EMT regulators were analyzed. Notably, all of the tested mRNAs were expressed at significantly higher levels in the tumors of *miR-34a/b/c* knockout *Apc*$^{Min/+}$ mice. Therefore, our screen identified numerous additional miR-34a/b/c targets, which may be upregulated in colorectal cancer and relevant for tumor progression.

Next, we performed an exemplary characterization of *Wasf1* as a direct miR-34a/b/c target, because Wasf1 is known to regulate cancer-relevant processes (41). A luciferase-based reporter

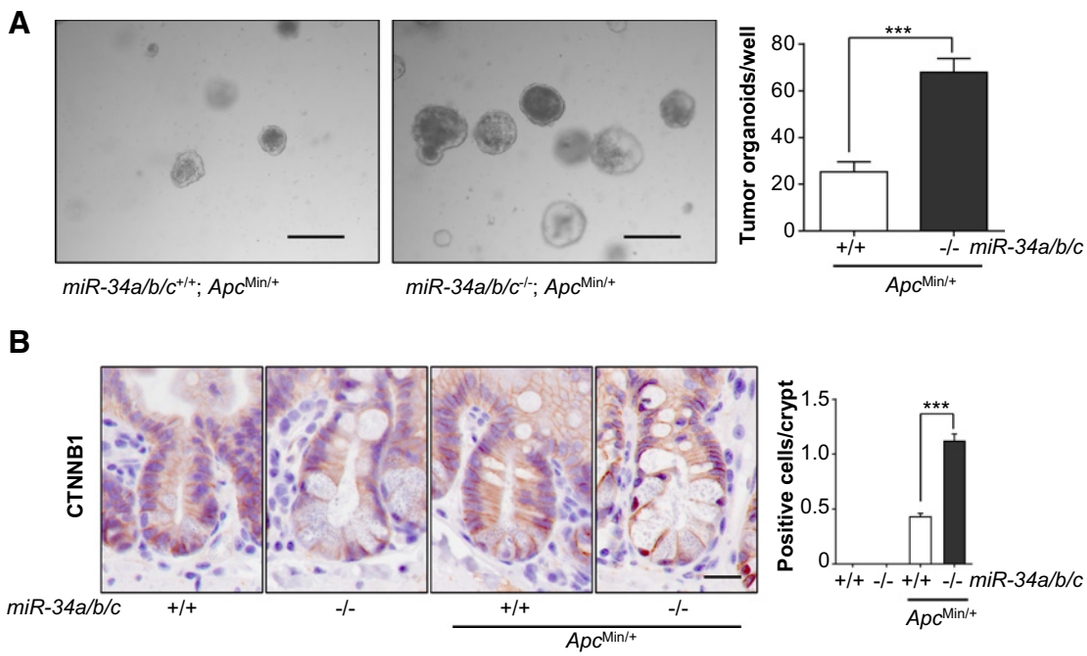

Figure 5.

miR-34a/b/c loss enhances intestinal tumor organoid formation and Wnt signaling. **A,** Tumor organoid formation assay of adenomas (three tumors per mice) from mice with the indicated genotypes ($n = 2$ mice per genotype). Scale bar, 200 μm. **B,** Detection of β-catenin localization. The number of nuclear β-catenin-positive cells was counted in ≥ 200 crypts ($n = 5$ mice per genotype). Scale bar, 20 μm. In **A–B**, results are presented as mean ± SEM. ***, $P < 0.001$ (Student t test).

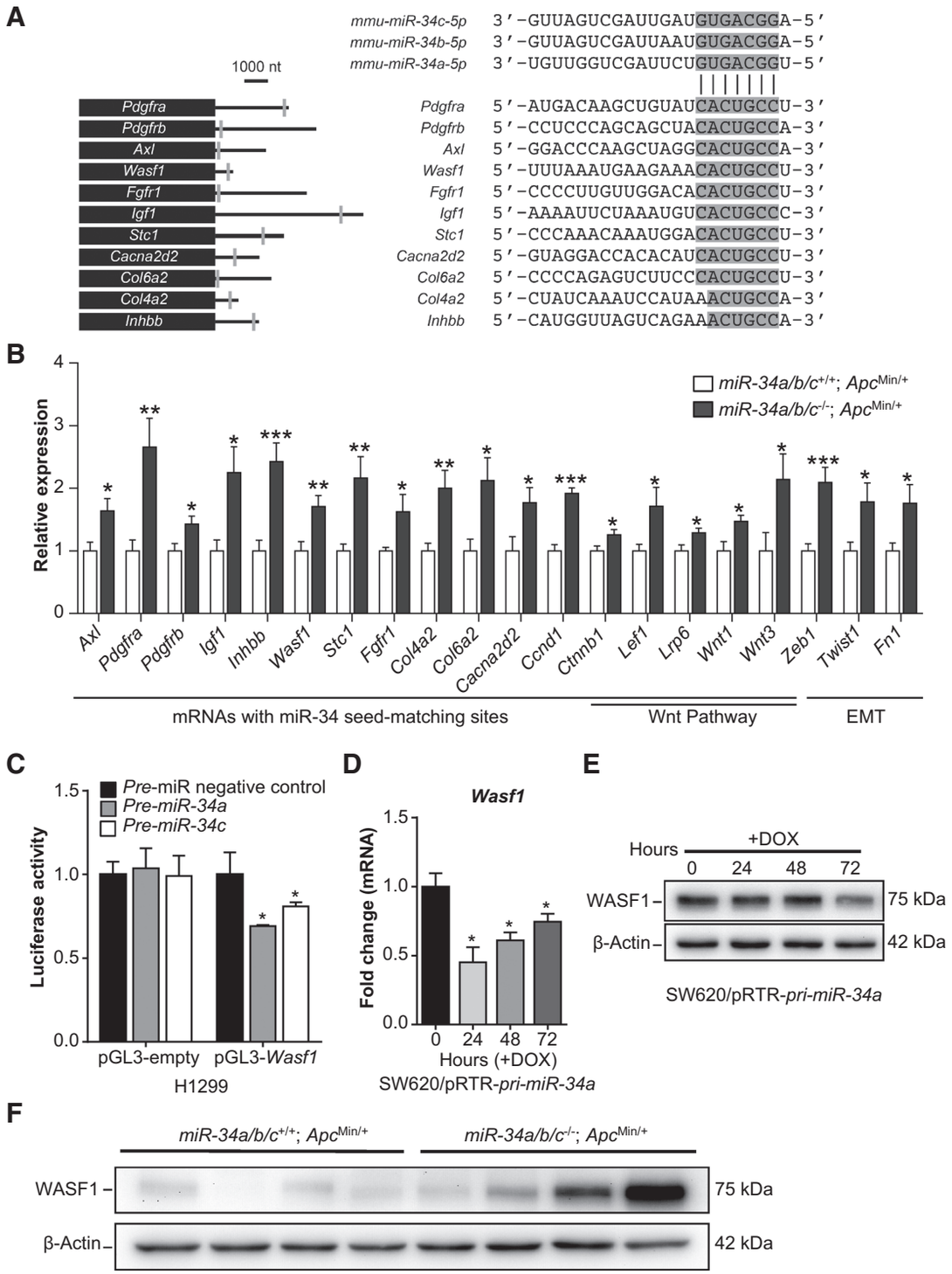

Figure 6.

Validation and characterization of upregulated miR-34a/b/c target mRNAs. **A,** Positions of miR-34 seed-matching sequences (gray vertical bars) within selected mRNAs (left panel). 3′-UTR sequences of the miR-34 binding site of the selected mRNAs are given in 5′- to 3′-orientation (right panel). **B,** mRNA expression of selected genes in tumors from mice with the indicated genotypes (three tumors per mouse) were determined by qPCR ($n = 3$ mice per genotype). **C,** Dual reporter assay in H1299 cells cotransfected with *pre-miR-34a* mimics, *pre-miR-34c* mimics or control oligonucleotides and *Wasf1* 3′-UTR-reporter constructs ($n = 3$). **D,** Detection of *Wasf1* mRNA by qPCR after addition of DOX for the indicated periods to SW620/pRTR-*pri-miR-34a* cells ($n = 3$). **E,** Western blot analysis of WASF1 after activation of ectopic *pri-miR-34a* expression for the indicated periods in SW620/pRTR-*pri-miR-34a* cells ($n = 3$). **F,** Western blot analysis of WASF1 expression in tumors from *miR-34a/b/c*$^{-/-}$; *Apc*$^{Min/+}$ mice or *miR-34a/b/c*$^{+/+}$; *Apc*$^{Min/+}$ mice ($n = 4$ mice per genotype). In **B–D**, results are presented as mean ± SD. *, $P < 0.05$; **, $P < 0.01$; ***, $P < 0.001$ (Student t test).

containing the full-length 3′-UTR of the murine *Wasf1* mRNA was significantly repressed by cotransfection of *pre-miR-34a* or *pre-miR-34c* (Fig. 6C). In addition, we detected a significant reduction of *Wasf1* mRNA expression after ectopic expression of *pri-miR-34a* in SW620 colorectal cancer cells (Fig. 6D). The WASF1 protein showed a delayed repression 72 hours after activation of the *pri-miR-34a* allele, which may be due to an unusually stable WASF1 protein (Fig. 6E). Consistent with being a miR-34a/b/c target, the WASF1 protein showed increased expression in three out of four tumors isolated from *miR-34a/b/c* knockout $Apc^{Min/+}$ mice, when compared with miR-34a/b/c-proficient tumors (Fig. 6F). Taken together, these results show that *Wasf1* is a direct target of miR-34a/b/c.

Increased expression of miR-34a/b/c targets in human colorectal cancers is associated with poor survival

In order to determine whether the miR-34 targets described above are also clinically relevant, we analyzed their expression within the expression profiles of 460 human colorectal adenocarcinomas deposited in TCGA database (30). Interestingly, *INHBB*, *PDGFRB*, *STC1*, and *COL4A2* showed a significantly elevated expression in primary colorectal cancers (Fig. 7A). Furthermore, a significantly increased expression of *INHBB*, *AXL*, *FGFR1*, and *PDGFRB* was detected in primary colorectal cancers from patients with nodal status N2 when compared with samples from patients with lower nodal status (Fig. 7B). Except for *AXL*, a significantly increased expression of these mRNAs was associated with an increased tumor stage (Supplementary Fig. S6A). In addition, increased expression of *INHBB* and *AXL* in primary colorectal cancers was significantly associated with decreased patient survival (Fig. 7C; Supplementary Table S5). Elevated expression of *COL4A2*, *WASF1*, *STC1*, and *PDGFRB* was also associated with poor survival, although not significantly (Supplementary Fig. S6B). Because poor survival is mostly due to metastatic spread, these results suggest that the elevated expression of these mRNAs, which may be due to loss of *miR-34a/b/c*, promotes metastasis.

Finally, we compiled the regulations identified here and combined them with previously published results on miR-34a/b/c-regulated pathways in a summarizing model shown in Fig. 7D. Notably, several of the miR-34 targets displaying elevated expression after *miR-34a/b/c* deletion are involved in transmembrane signal transductions, which also activate the Wnt signaling pathway by inhibition of GSK-3β. Taken together, miR-34a/b/c presumably suppresses intestinal tumorigenesis caused by loss of *Apc* by downregulating the expression of a large number of protumorigenic factors. In case *miR-34a/b/c* expression is lost or silenced during tumor progression, these pathways may be further activated and thereby contribute to colorectal cancer progression.

Discussion

The increase in the pool of intestinal stem cells (ISC) in the *miR-34a/b/c*-deficient mice observed here may underlie the increased rate of tumor formation in $Apc^{Min/+}$ mice, because ISC were shown to serve as efficient tumor initiating cells during intestinal tumorigenesis (38). Paneth cells provide a niche for ISCs and communicate with these via multiple signaling pathways, among them the Delta/NOTCH and Wnt/APC/β-catenin pathways, which are under negative control by miR-34a/b/c (15, 37): that is, several key components of the Wnt signaling pathway are miR-34a/b/c targets (WNT1, WNT3, LRP6, LEF1, and β-catenin (37, 40). Moreover, GSK-3β, which phosphorylates β-catenin and thereby leads to its poly-ubiquitination and proteasomal degradation, is inhibited by the PKB/AKT and PI3K pathways, which are also under control of miR-34a/b/c. Therefore, the concerted deregulation of the NOTCH and WNT pathways caused by the loss of *miR-34a/b/c* is a likely cause for the increased number of Paneth and stem cells. In support of this scenario, we also noticed an increased tumor organoid formation rate in *miR-34a/b/c*$^{-/-}$; $Apc^{Min/+}$ adenomas as well as an increased accumulation of nuclear β-catenin in the untransformed, epithelial cells of intestinal crypts in *miR-34a/b/c*-deficient $Apc^{Min/+}$ mice. In addition, a recent study suggests that activation of the Wnt/β-catenin pathway correlates with T-cell exclusion (42). Therefore, miR-34 may regulate immune responses through Wnt signaling. In addition, the expression of barrier proteins was decreased in *miR-34a/b/c*$^{-/-}$; $Apc^{Min/+}$ mice (e.g., *Muc1*, *Tff3*, and *Retnlb*). In combination with the decreased presence of immune cells, these effects of *miR-34a/b/c* loss may contribute, at least in part, to the increased bacterial infiltration observed in *miR-34a/b/c*$^{-/-}$; $Apc^{Min/+}$ adenomas.

In addition, we found that the deletion of *miR-34a/b/c* in adenomas leads to the upregulation of previously described miR-34a/b/c target mRNAs, such as *Pdgfra*, *Pdgfrb*, and *Axl*, which are known to enhance colorectal cancer formation (43). Furthermore, a set of novel, putative miR-34a/b/c target mRNAs (*Wasf1*, *Fgfr1*, *Igf1*, *Stc1*, *Cacna2d2*, *Col6a2*, *Col4a2*, and *Inhbb*), which were reported to be involved in tumorigenesis (41, 44–49), was upregulated in *miR-34a/b/c*-deficient adenomas. The factors encoded by these genes form complex signaling and functional networks (see also Fig. 7D): PDGFRA, PDGFRB, FGFR1, AXL, and IGF1, which are either ligands or receptors of the tyrosine kinase family, activate the PI3K and MAPK signaling pathway, and thereby promote cell growth, survival, EMT, and metastasis. Notably, CACNA2D2, a voltage-dependent calcium channel, deregulates calcium homeostasis when ectopically expressed (47). The resulting calcium release may induce the activation of PKB/AKT and RAS to promote cell proliferation and angiogenesis (47). INHBB assembles into activins, which are critical modulators of growth and survival (49). COL4A2 is a major structural protein of the basement membrane and COL6A2 has an anchoring function. Both collagens stimulate integrin signaling and are involved in cell growth, angiogenesis, and tumor metastasis (48). WASF1, a new miR-34a/b/c target characterized here, mediates actin polymerization, lamellipodia formation, and plays a critical role in cancer cell migration and invasion (41). STC1 is an endocrine regulator of calcium and phosphate homeostasis, which promotes cell proliferation and inhibits apoptosis through CCND1 and CDK2/4 (50). Taken together, miR-34a/b/c presumably act as global regulators to fine tune multiple cellular functions, which are necessary for the homeostasis of intestinal epithelia. Because miR-34a has been shown to form bimodal switches with at least some of its targets (15), the loss of miR-34a/b/c during colorectal cancer progression may have significant effects on the regulation of these signaling and expression networks, which ultimately promote intestinal tumorigenesis. miR-34a/b/c have a multitude of targets in intestinal epithelial and colon cancer cells as shown here and in previous studies (10). Therefore, it seems plausible that the effects of miR-34a/b/c loss are mediated by the combined activity of multiple upregulated targets and not by one or a few targets.

A subset of the direct targets of miR-34a/b/c may significantly contribute to human colorectal tumorigenesis because their

elevated expression was associated with poor clinical outcomes of colorectal cancer patients. However, further analysis will be necessary to corroborate the role of *miR-34a/b/c* silencing for their increased expression in colorectal tumors. Our results suggest that miR-34 mimetics may be used to target multiple key pathways simultaneously and could thereby potentially prevent the

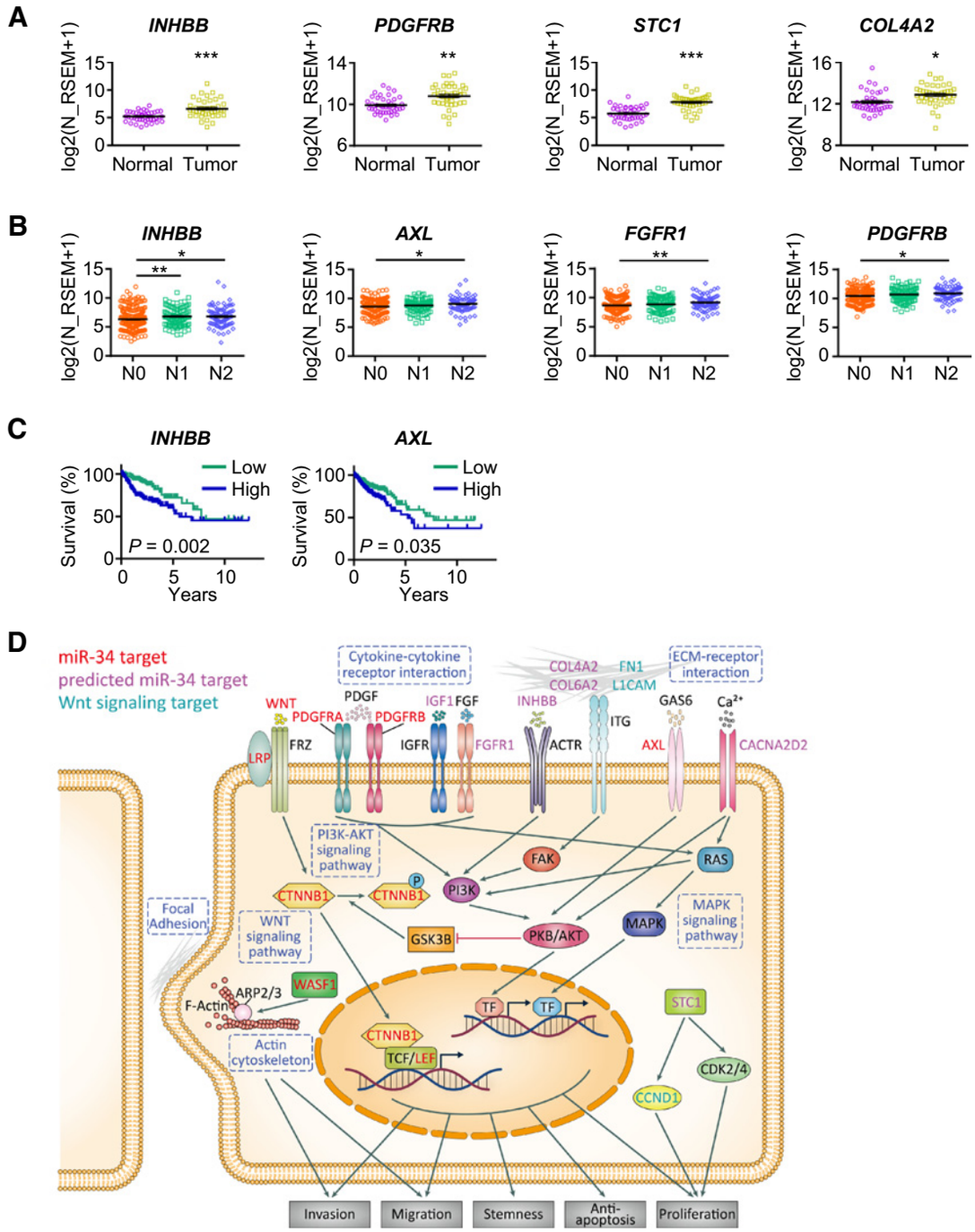

Figure 7.

Analysis of miR-34 target expression and clinical associations in the TCGA-COAD database. Correlative analysis of mRNA expression in the TCGA-COAD database. **A,** Expression of selected miR-34 targets in tumor and matched normal tissue in the TCGA collection of COAD ($n = 41$ patients). **B,** Correlation of mRNA expression with nodal status ($n = 460$ patients). **C,** Kaplan–Meier analysis of overall survival ($n = 306$ patients). Results were compared with a log-rank test. **D,** Summarizing model of regulations and signal transduction events activated by deletion of *miR-34a/b/c* in $Apc^{Min/+}$ mice identified in this study. Selected published (red) and predicted (purple) miR-34a/b/c target genes, as well as WNT-regulated factors (cyan) are depicted. In **A–B**, results are presented as mean ± SEM. *, $P < 0.05$; **, $P < 0.01$; ***, $P < 0.001$ (Student *t* test).

emergence of resistance caused by mutations of single pathways. Therefore, miR-34a/b/c replacement therapy may represent a potential option for the treatment of colorectal cancer.

Disclosure of Potential Conflicts of Interest

No potential conflicts of interest were disclosed.

Authors' Contributions

Conception and design: H. Hermeking
Acquisition of data (provided animals, acquired and managed patients, provided facilities, etc.): L. Jiang, H. Hermeking
Analysis and interpretation of data (e.g., statistical analysis, biostatistics, computational analysis): L. Jiang, H. Hermeking
Writing, review, and/or revision of the manuscript: L. Jiang, H. Hermeking
Study supervision: H. Hermeking
Other (experimental design): L. Jiang

Acknowledgments

We are grateful to Alexander Nikitin for providing *miR-34b/c*$^{fl/fl}$ mice, Marlon Schneider for *Apc*$^{Min/+}$ mice, Hans Clevers for the *Olfm4* plasmid, Matjaz Rokavec for initial help with setting up the *Apc*$^{Min/+}$ mouse cohorts, and Markus Kaller for advice on bioinformatics analyses. We would also like to thank Peter Jung for discussions and Ursula Götz for technical assistance.

Grant Support

H. Hermeking received support from a Deutsche Krebshilfe Grant (No. 109531) and the Rudolf Bartling Stiftung (V/124). L. Jiang received a fellowship from the China Scholarship Council.

The costs of publication of this article were defrayed in part by the payment of page charges. This article must therefore be hereby marked *advertisement* in accordance with 18 U.S.C. Section 1734 solely to indicate this fact.

Received August 8, 2016; revised October 4, 2016; accepted March 23, 2017; published OnlineFirst March 31, 2017.

References

1. Siegel RL, Miller KD, Jemal A. Cancer statistics, 2016. CA Cancer J Clin 2016;66:7–30.
2. Kinzler KW, Vogelstein B. Lessons from hereditary colorectal cancer. Cell 1996;87:159–70.
3. Bienz M, Clevers H. Linking colorectal cancer to Wnt signaling. Cell 2000;103:311–20.
4. Moser AR, Mattes EM, Dove WF, Lindstrom MJ, Haag JD, Gould MN. ApcMin, a mutation in the murine Apc gene, predisposes to mammary carcinomas and focal alveolar hyperplasias. Proc Natl Acad Sci U S A 1993;90:8977–81.
5. Luongo C, Moser AR, Gledhill S, Dove WF. Loss of Apc+ in intestinal adenomas from Min mice. Cancer Res 1994;54:5947–52.
6. Moser AR, Luongo C, Gould KA, McNeley MK, Shoemaker AR, Dove WF. ApcMin: a mouse model for intestinal and mammary tumorigenesis. Eur J Cancer 1995;31A:1061–4.
7. Vogelstein B, Lane D, Levine AJ. Surfing the p53 network. Nature 2000; 408:307–10.
8. Hermeking H.MicroRNAs in the p53 network: micromanagement of tumour suppression. Nat Rev Cancer 2012;12:613–26.
9. Hunten S, Kaller M, Drepper F, Oeljeklaus S, Bonfert T, Erhard F, et al. p53-Regulated networks of protein, mRNA, miRNA, and lncRNA expression revealed by integrated pulsed stable isotope labeling with amino acids in cell culture (pSILAC) and next generation sequencing (NGS) analyses. Mol Cell Proteomics 2015;14:2609–29.
10. Rokavec M, Li H, Jiang L, Hermeking H. The p53/miR-34 axis in development and disease. J Mol Cell Biol 2014;6:214–30.
11. Hermeking H.p53 enters the microRNA world. Cancer Cell 2007;12: 414–8.
12. Tarasov V, Jung P, Verdoodt B, Lodygin D, Epanchintsev A, Menssen A, et al. Differential regulation of microRNAs by p53 revealed by massively parallel sequencing: miR-34a is a p53 target that induces apoptosis and G1-arrest. Cell Cycle 2007;6:1586–93.
13. Siemens H, Jackstadt R, Hunten S, Kaller M, Menssen A, Gotz U, et al. miR-34 and SNAIL form a double-negative feedback loop to regulate epithelial-mesenchymal transitions. Cell Cycle 2011;10:4256–71.
14. Liu C, Kelnar K, Liu B, Chen X, Calhoun-Davis T, Li H, et al. The microRNA miR-34a inhibits prostate cancer stem cells and metastasis by directly repressing CD44. Nat Med 2011;17:211–5.
15. Bu P, Wang L, Chen KY, Srinivasan T, Murthy PK, Tung KL, et al. A miR-34a-numb feedforward loop triggered by inflammation regulates asymmetric stem cell division in intestine and colon cancer. Cell Stem Cell 2016;18: 189–202.
16. Cheng CY, Hwang CI, Corney DC, Flesken-Nikitin A, Jiang L, Oner GM, et al. miR-34 cooperates with p53 in suppression of prostate cancer by joint regulation of stem cell compartment. Cell Rep 2014;6:1000–7.
17. Choi YJ, Lin CP, Ho JJ, He X, Okada N, Bu P, et al. miR-34 miRNAs provide a barrier for somatic cell reprogramming. Nat Cell Biol 2011;13:1353–60.
18. Lodygin D, Tarasov V, Epanchintsev A, Berking C, Knyazeva T, Korner H, et al. Inactivation of miR-34a by aberrant CpG methylation in multiple types of cancer. Cell cycle 2008;7:2591–600.
19. Siemens H, Neumann J, Jackstadt R, Mansmann U, Horst D, Kirchner T, et al. Detection of miR-34a promoter methylation in combination with elevated expression of c-Met and β-catenin predicts distant metastasis of colon cancer. Clin Cancer Res 2013;19:710–20.
20. Adams BD, Parsons C, Slack FJ. The tumor-suppressive and potential therapeutic functions of miR-34a in epithelial carcinomas. Expert Opin Ther Targets 2016;20:737–53.
21. Rokavec M, Oner MG, Li H, Jackstadt R, Jiang L, Lodygin D, et al. IL-6R/STAT3/miR-34a feedback loop promotes EMT-mediated colorectal cancer invasion and metastasis. J Clin Invest 2014;124:1853–67.
22. Gregorieff A, Clevers H. In situ hybridization to identify gut stem cells. Curr Protoc Stem Cell Biol 2010;Chapter 2:Unit 2F 1.
23. Risso D, Ngai J, Speed TP, Dudoit S. Normalization of RNA-seq data using factor analysis of control genes or samples. Nat Biotechnol 2014;32:896–902.
24. Kallio MA, Tuimala JT, Hupponen T, Klemela P, Gentile M, Scheinin I, et al. Chipster: user-friendly analysis software for microarray and other high-throughput data. BMC Genom 2011;12:507.
25. Huang da W, Sherman BT, Lempicki RA. Bioinformatics enrichment tools: paths toward the comprehensive functional analysis of large gene lists. Nucleic Acids Res 2009;37:1–13.
26. Subramanian A, Tamayo P, Mootha VK, Mukherjee S, Ebert BL, Gillette MA, et al. Gene set enrichment analysis: a knowledge-based approach for interpreting genome-wide expression profiles. Proc Natl Acad Sci U S A 2005;102:15545–50.
27. Lewis BP, Burge CB, Bartel DP. Conserved seed pairing, often flanked by adenosines, indicates that thousands of human genes are microRNA targets. Cell 2005;120:15–20.
28. Sato T, Stange DE, Ferrante M, Vries RG, Van Es JH, Van den Brink S, et al. Long-term expansion of epithelial organoids from human colon, adenoma, adenocarcinoma, and Barrett's epithelium. Gastroenterology 2011;141:1762–72.
29. Livak KJ, Schmittgen TD. Analysis of relative gene expression data using real-time quantitative PCR and the 2(-Delta Delta C(T)) Method. Methods 2001;25:402–8.
30. Cancer Genome Atlas N. Comprehensive molecular characterization of human colon and rectal cancer. Nature 2012;487:330–7.
31. Vogt M, Munding J, Gruner M, Liffers ST, Verdoodt B, Hauk J, et al. Frequent concomitant inactivation of miR-34a and miR-34b/c by CpG methylation in colorectal, pancreatic, mammary, ovarian, urothelial, and renal cell carcinomas and soft tissue sarcomas. Virchows Arch 2011;458:313–22.
32. Lee SH, Hu LL, Gonzalez-Navajas J, Seo GS, Shen C, Brick J, et al. ERK activation drives intestinal tumorigenesis in Apc(min/+) mice. Nat Med 2010;16:665–70.
33. Love MI, Huber W, Anders S. Moderated estimation of fold change and dispersion for RNA-seq data with DESeq2. Genome Biol 2014;15:550.
34. Robinson MD, McCarthy DJ, Smyth GK. edgeR: a Bioconductor package for differential expression analysis of digital gene expression data. Bioinformatics 2010;26:139–40.

35. Munoz J, Stange DE, Schepers AG, van de Wetering M, Koo BK, Itzkovitz S, et al. The Lgr5 intestinal stem cell signature: robust expression of proposed quiescent `+4' cell markers. EMBO J 2012;31:3079–91.
36. Merlos-Suarez A, Barriga FM, Jung P, Iglesias M, Cespedes MV, Rossell D, et al. The intestinal stem cell signature identifies colorectal cancer stem cells and predicts disease relapse. Cell Stem Cell 2011;8:511–24.
37. Kim NH, Kim HS, Kim N-G, Lee I, Choi H-S, Li X-Y, et al. p53 and miRNA-34 are Suppressors of Canonical Wnt Signaling. Sci Signal 2011;4:ra71.
38. Barker N, Ridgway RA, van Es JH, van de Wetering M, Begthel H, van den Born M, et al. Crypt stem cells as the cells-of-origin of intestinal cancer. Nature 2009;457:608–11.
39. Garofalo M, Jeon YJ, Nuovo GJ, Middleton J, Secchiero P, Joshi P, et al. MiR-34a/c-Dependent PDGFR-alpha/beta downregulation inhibits tumorigenesis and enhances TRAIL-Induced apoptosis in lung cancer. PloS One 2013;8:e67581.
40. Kaller M, Liffers S-T, Oeljeklaus S, Kuhlmann K, Röh S, Hoffmann R, et al. Genome-wide characterization of miR-34a induced changes in protein and mRNA expression by a combined pulsed SILAC and microarray analysis. Mol Cell Proteo 2011;10:M111. 010462.
41. Zhang J, Zhou S, Tang L, Shen L, Xiao L, Duan Z, et al. WAVE1 gene silencing via RNA interference reduces ovarian cancer cell invasion, migration and proliferation. Gynecol Oncol 2013;130:354–61.
42. Corrales L, Matson V, Flood B, Spranger S, Gajewski TF. Innate immune signaling and regulation in cancer immunotherapy. Cell Res 2016; 27:96–108.
43. Craven RJ, Xu LH, Weiner TM, Fridell YW, Dent GA, Srivastava S, et al. Receptor tyrosine kinases expressed in metastatic colon cancer. Int J Cancer 1995;60:791–7.
44. Grose R, Dickson C. Fibroblast growth factor signaling in tumorigenesis. Cytokine Growth Factor Rev 2005;16:179–86.
45. OlivoMarston SE, Hursting SD, Lavigne J, Perkins SN, Maarouf RS, Yakar S, et al. Genetic reduction of circulating insulinlike growth factor1 inhibits azoxymethaneinduced colon tumorigenesis in mice. Mol Carcinogen 2009;48:1071–6.
46. Tamura S, Oshima T, Yoshihara K, Kanazawa A, Yamada T, Inagaki D, et al. Clinical significance of STC1 gene expression in patients with colorectal cancer. Anticancer Res 2011;31:325–9.
47. Warnier M, Roudbaraki M, Derouiche S, Delcourt P, Bokhobza A, Prevarskaya N, et al. CACNA2D2 promotes tumorigenesis by stimulating cell proliferation and angiogenesis. Oncogene 2015;34:5383–94.
48. Worthley DL, Giraud AS, Wang TC. The extracellular matrix in digestive cancer. Cancer Microenviron 2010;3:177–85.
49. Togashi Y, Kogita A, Sakamoto H, Hayashi H, Terashima M, de Velasco MA, et al. Activin signal promotes cancer progression and is involved in cachexia in a subset of pancreatic cancer. Cancer Lett 2015;356:819–27.
50. Du Y-Z, Gu X-H, Cheng S-F, Li L, Liu H, Hu L-P, et al. The oncogenetic role of stanniocalcin 1 in lung adenocarcinoma: a promising serum candidate biomarker for tracking lung adenocarcinoma progression. Tumor Biol 2015:1–12.